NANO LETTERS
Cite This: Nano Lett. 2018, 18, 2645−2649
Letter
pubs.acs.org/NanoLett

DNA-Mediated Size-Selective Nanoparticle Assembly for Multiplexed Surface Encoding

Qing-Yuan Lin,[†,‡,⊥] Edgar Palacios,[§,‡,⊥] Wenjie Zhou,[‡,∥] Zhongyang Li,[‡,§] Jarad A. Mason,[‡,∥] Zizhuo Liu,[‡,§] Haixin Lin,[‡,∥] Peng-Cheng Chen,[†,‡] Vinayak P. Dravid,[*,†,‡] Koray Aydin,[*,§,‡] and Chad A. Mirkin[*,†,‡,∥]

[†]Department of Materials Science and Engineering, [‡]International Institute for Nanotechnology, [§]Department of Electrical Engineering and Computer Science, and [∥]Department of Chemistry, Northwestern University, 2145 Sheridan Road, Evanston, Illinois 60208, United States

Supporting Information

ABSTRACT: Multiplexed surface encoding is achieved by positioning two different sizes of gold nanocubes on gold surfaces with precisely defined locations for each particle via template-confined, DNA-mediated nanoparticle assembly. As a proof-of-concept demonstration, cubes with 86 and 63 nm edge lengths are assembled into arrangements that physically and spectrally encrypt two sets of patterns in the same location. These patterns can be decrypted by mapping the absorption intensity of the substrate at λ = 773 and 687 nm, respectively. This multiplexed encoding platform dramatically increases the sophistication and density of codes that can be written using colloidal nanoparticles, which may enable high-security, high-resolution encoding applications.

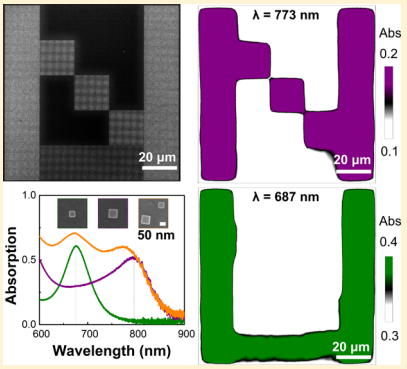

KEYWORDS: *Multiplexed encoding, DNA-mediated assembly, gold nanoparticles, gap mode, size-selective assembly*

Nanostructures have been utilized as encoding materials for a variety of applications, including biomolecular detection[1] and analysis,[2] clinical diagnostics[3] and tracking,[4] anticounterfeiting,[5] food quality and safety assessment,[6] and forensic marking.[7] Because of their small size, nanomaterials enable encoding with high density,[8] high crypticity,[9] high sensitivity,[10] and minimal influence on the host target.[11] Indeed, nanomaterials provide a pathway to design high-resolution, high density multiplexed platforms for high-security encoding.[5] Before this can be realized, however, new synthetic techniques are needed that allow multiple sizes, shapes, and/or compositions of colloidal nanoparticles to be assembled on surfaces with individual particle control.[12−15] Herein, we leverage template-confined, DNA-mediated nanoparticle assembly to position two different sizes of gold nanocubes on gold surfaces with precisely defined locations for each particle. Importantly, because different cube sizes give rise to different optical absorption spectra when positioned a fixed distance above a gold film, this size-selective assembly approach can be used for multiplexed surface encoding applications. As a proof-of-concept demonstration, cubes with 86 and 63 nm edge lengths are assembled into patterns that physically and spectrally encrypt two sets of patterns in the same location. Through reflectivity spectroscopy and finite-difference time-domain (FDTD) simulations, we find that these patterns can be decrypted by mapping the absorption intensity of the substrate at different wavelengths. This multiplexed encoding platform dramatically increases the sophistication and density of codes that can be written using colloidal nanoparticles, which should enable high-security, high-resolution encoding applications.

Over the past few decades, a diverse range of nanoscale architectures, such as nanowires,[16] nanodisks,[17] nanorods,[18] and nanopillars,[19] have been designed and synthesized to rationally encode information through optical signals[18,20] such as luminescence[16,21] and fluorescence.[22] Colloidal nanoparticles represent a particularly appealing class of materials for encoding applications, because they can be synthesized in many different sizes, shapes, and compositions at large scale[23−25] and can be manipulated through colloidal chemistry to achieve desired properties.[26,27] For example, when colloidal metal nanocubes are positioned a fixed distance above a metal film, a plasmonic gap mode emerges that allows for tunable absorption and emission.[12,28,29] The resonance of the cavity mode is dictated by the size of the particle[30] as well as the size of the gap between the nanoparticle and surface,[31] making it an ideal system for surface encoding at tunable wavelengths.[14] Despite these advantages, using colloidal particles for high-resolution multiplexed encoding, an attractive approach to increasing the complexity and information content of codes and, therefore, the difficulty of counterfeiting[11,16,19−21] through the incorpo-

Received: February 5, 2018
Revised: March 15, 2018
Published: March 23, 2018

DOI: 10.1021/acs.nanolett.8b00509
Nano Lett. 2018, 18, 2645−2649

ration of multiple codes within a single platform, has proven challenging due to a lack of synthetic approaches for positioning of multiple nanoparticles that differ in size on a surface with single-particle resolution.

Recent approaches that combine top-down patterning and bottom-up colloidal assembly point toward the possibility of assembling multiple particles, which differ in size, at precise locations on surfaces.[14,32,33] For example, DNA-mediated assembly allows one to precisely control the interactions both between nanoparticles and between nanoparticles and a surface in a highly specific manner. Moreover, through the choice of oligonucleotide sequence and length one can systematically tune interaction strength and interparticle distance.[34−36] Indeed, DNA has been used as a surface ligand to program the assembly of vertical stacks of nanoparticles on surfaces,[12,13,37−40] enabling the creation of entirely new classes of optical materials. Importantly, in the case of DNA-driven processes, this control has been limited to the surface normal (generating one-dimensional stacks). In addition, capillary-driven nanoparticle assembly has been used to position individual particles into lithographically defined patterns[15,41−43] but this approach is limited to the assembly of only one type of nanoparticle on a given substrate. To date, the ability to robustly immobilize different-sized sub-100 nm nanoparticles with independent control over the location of every individual particle has not been realized.[43−45] If this limitation could be overcome, one could literally optically program a substrate with information that is encoded in the patterns of the nanoparticles.

Herein, we report the realization of a novel multiplexed surface encoding technique based upon the size-selective, DNA-mediated assembly of nanoparticles. By using a polymer template to provide size selectivity, two types of gold nanocubes, which differ in size, were assembled on a gold substrate at precisely defined locations. Since the resonance wavelengths of the plasmonic gap modes depend on the size of the cubes, we can encode the surface by patterning cubes that have a specific size and decode the information by measuring the intensity of absorption at the corresponding gap mode wavelength, allowing one to encode multiple sets of patterns on the same area. As a proof-of-concept example, we encoded two superimposed patterns consisting of either the letter "N" or the letter "U" and show that the encoded information can be decoded by measuring the absorption intensity map of the surface at the representative resonance wavelengths of the two different gap modes. Broadly, this method provides a high level of structural control for multicomponent nanoparticle assembly on surfaces with single particle resolution, and it creates a tunable platform for high-resolution multiplexed surface encoding.

In a typical experiment to construct encoded surfaces, two different sizes of gold nanocubes were assembled onto substrates in a stepwise manner via template-confined, DNA-mediated assembly (Figure 1a). Specifically, electron beam lithography (EBL) was used to pattern 100 nm thick poly(methyl methacrylate) (PMMA) pores of two different diameters at defined locations on gold-coated Si substrates, such that the bottom of each pore consisted of exposed gold. As has been previously reported,[12] the nanoparticles and the exposed gold in the pores were densely functionalized with 3′-propylthiolated DNA and hybridized with complementary linker strands. Then, the nanoparticles were assembled within the pores by designing the DNA on the gold surface to be complementary to the DNA on the nanoparticles (DNA

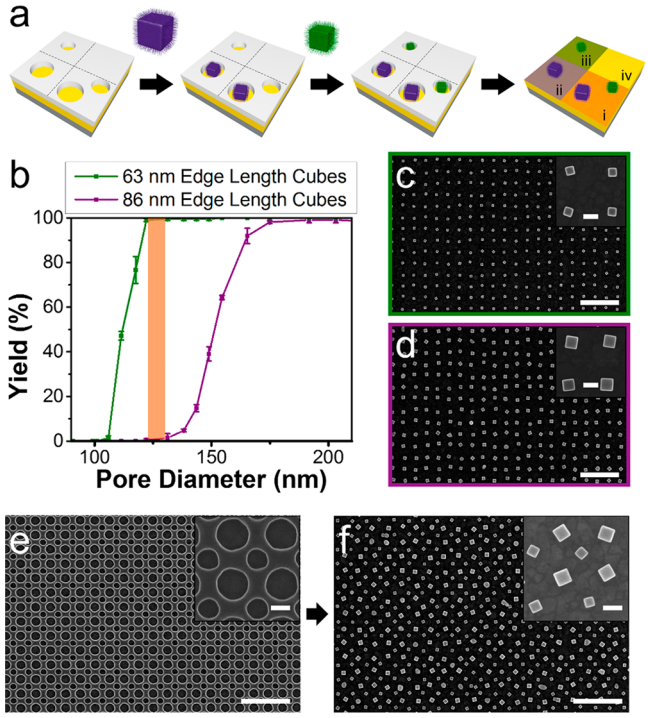

Figure 1. Assembly of two sizes of gold nanocubes on gold substrates at precisely defined locations. (a) Scheme showing the stepwise DNA-mediated size-selective nanoparticle assembly. Two different sizes of polymer pores were used to assemble large (purple) and small (green) cubes into four types of encoding pixels on the surface. (b) The assembly yield as a function of pore diameter for cubes with 86 and 63 nm edge lengths. The yield curves clearly show the size-selective behavior of the template-confined assembly with a range of pore sizes (orange shade) that result in high yield of small cube assembly and low yield of large cube assembly. (c−f) SEM images of an array of (c) 63 nm edge length cubes assembled in 130 nm diameter pores, (d) 86 nm edge length cubes assembled in 200 nm diameter pores, (e) polymer pores with 130 and 200 nm diameter pores, and (f) cubes with 63 and 86 nm edge lengths assembled in the polymer template shown in panel e. All arrays have a periodicity of 300 nm. The scale bars are 1 μm for the large images and 100 nm for the insets.

sequences are specified in Table S1 of the Supporting Information). The sizes of the pores were deliberately designed such that larger cubes can only fit inside the larger set of pores, while the smaller cubes can fit into both sizes of pores. Therefore, the larger set of pores was first filled by immersing the substrate in a solution containing only the larger cubes. After assembly, cubes not attached to the surface were removed by rinsing with buffer solution. Subsequently, the smaller set of pores was filled by performing a second assembly with the smaller cubes. After assembly, the PMMA template was dissolved without significantly disturbing the location of the assembled nanoparticles.[46] Finally, the nanoparticle arrays were either transferred back to buffer solution for optical characterization, or dried for characterization by scanning electron microscopy (SEM). Note that although EBL combined with metal deposition and lift-off may be used to create similar patterns, the structures demonstrated here are fundamentally different from those fabricated only through top-down lithography.

One advantage of our approach is the ability to position single crystalline metallic nanoparticles of different sizes on surfaces, which is extremely difficult, if not impossible to do

DOI: 10.1021/acs.nanolett.8b00509
Nano Lett. 2018, 18, 2645−2649

with EBL. In addition to generating polycrystalline structures with inferior optical properties, EBL is unable to make structures with different heights on this scale. Additionally, our approach provides chemical differentiation of particle building blocks based upon DNA sequence. Importantly, others will be able to extend what we report here to a myriad of colloidal materials, as long as they can be modified with DNA. Finally, our method can be scaled with other higher throughput techniques that allow the direct patterning of DNA such as polymer pen lithography, which is also not possible using EBL.

To experimentally evaluate this size-selective assembly of nanocubes, single crystalline gold cubes with an average edge length of 86 ± 3 and 63 ± 2 nm were synthesized[25] and functionalized with propylthiolated DNA (Supporting Information, Figure S1).[12] To determine the optimal pore sizes for stepwise assembly, we explored how the assembly yield was affected by pore diameter ranging from 90 to 280 nm for both sizes of cubes. As shown in Figure 1b, 63 nm cubes required pore diameters larger than 120 nm for assembly to occur at high yield, while 86 nm cubes required pore diameters of at least 170 nm. The appropriate selection of pore diameters allowed gold cubes with both sizes to assemble into ordered arrays with >99% yield over an area of 100 by 100 μm (Figure 1c,d, Figure S2, experimental details of assembly are specified in the Supporting Information). The relationship between yield, pore size, and nanoparticle size allowed us to determine that pores of 125−135 nm in diameter resulted in both a high yield of assembled 63 nm cubes (>99%) and a low yield of assembled 86 nm cubes (<2%), making this pore size range ideal for the selective assembly of 63 nm cubes. Using a small pore size of 130 nm and a large pore size of 200 nm (Figure 1e) thus afforded the successful assembly of cubes with 63 and 86 nm edge lengths, respectively (Figure 1f).

Importantly, the ability to independently place two different-sized nanocubes on a single surface serves as a novel platform for multiplexed surface encoding. For the encoded surfaces reported here, the presence of a nanocube at a specific position on the gold surface will determine whether or not significant light is absorbed at the gap mode resonance wavelength, effectively serving as a bit of information (Figure 2a,b). Because the resonance wavelength depends on the edge length of the cube at a constant gap length of 10 nm (Figure 2c), the assembly of multiple sizes of cubes on a substrate allows for multiplexed surface encoding at multiple resonance wavelengths. Indeed, four types of encoding pixels, each 300 by 300 nm, can be generated with predetermined arrangements: (i) a pixel with both a large and a small cube, (ii) a pixel with only a large cube, (iii) a pixel with only a small cube, and (iv) a pixel with no cubes (Figure 1a). These encoding pixels were experimentally synthesized and used to encode two sets of patterns on substrates with single particle resolution (Supporting Information, Figure S3).

In order to confirm that these pixels encode the surface at multiple wavelengths, FDTD simulations were performed to test the strength of coupling between two gap modes when they are placed in close proximity to each other. Figure 2d shows the simulated absorption spectra of pixel types I (both 86 and 63 nm cubes on gold surface), ii (86 nm cubes on gold surface), and iii (63 nm cubes on gold surface), whereas the absorption spectrum of pixel type iv (gold surface without cubes) is shown in Figure 2b as the "off" state. Pixel type (i) is predicted to exhibit two absorption peaks with resonance wavelengths that are well-matched to the absorption spectra of

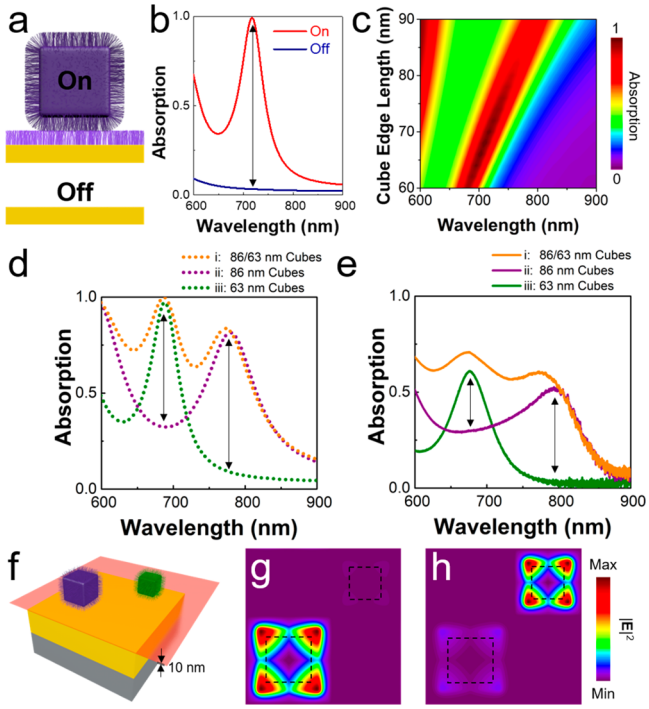

Figure 2. Multiplexed surface encoding with absorption intensity contrast at multiple wavelengths. (a) Schematics of a DNA-functionalized gold cube on a gold substrate through DNA hybridization (the "on" state) and a bare gold surface (the "off" state). (b) Simulated optical spectra showing the large absorption difference at the gap mode resonance when the cube is on or off the surface. The edge length of cube is 70 nm. (c) Simulated absorption spectra of cube arrays on gold surfaces as a function of the cube edge length. (d) Simulated and (e) measured absorption spectra of three types of encoding pixels: 63 nm edge length cubes (green), 86 nm edge length cubes (purple), and a mixture of the two (orange). The double arrows indicate the large absorption contrast between the two different size cubes. (f) Schematic of an encoding pixel that contains two different size cubes with a cross-section plane within the gap (gap plane with a thickness of 10 nm highlighted in red). (g-h) Simulated electric field profile of the sample along the cross-section plain at (g) λ = 773 nm and (h) λ = 687 nm.

pixels (ii) and (iii), indicating that there is very little coupling between the two gap modes. Moreover, absorption at the two gap mode resonance wavelengths displays a large contrast based on whether the cube is on or off the surface, making it possible to use absorption intensity to decode surface patterns.

The orthogonality of the two encoding gap modes was further explored by looking at the electric field profiles of a surface with both sizes of cubes at their respective resonance wavelengths. Figure 2f shows a cross-sectional plane (red plane) halfway between the gap of a unit cell from which the electric field profiles were taken. As evidenced by the electric field profile at λ = 773 nm (Figure 2g), only the gap between the 86 nm cube and the gold surface has strong electric field enhancement, leading to strong absorption at this gap mode resonance. At λ = 687 nm (Figure 2h), the gap between the 63 nm cube and the gold surface has a much stronger electric field enhancement. These results further confirmed that the two gap modes function independently. The predicted optical response was experimentally confirmed by measuring the absorption spectra of surfaces consisting of pixel types (i)−(iii) using pixel (iv) (gold surface) as the reference while the samples were immersed in a buffer solution (Figure 2e).

DOI: 10.1021/acs.nanolett.8b00509
Nano Lett. 2018, 18, 2645−2649

As a proof-of-concept example, we designed a surface pattern with two images encrypted, as shown in Figure 3a and 3b.

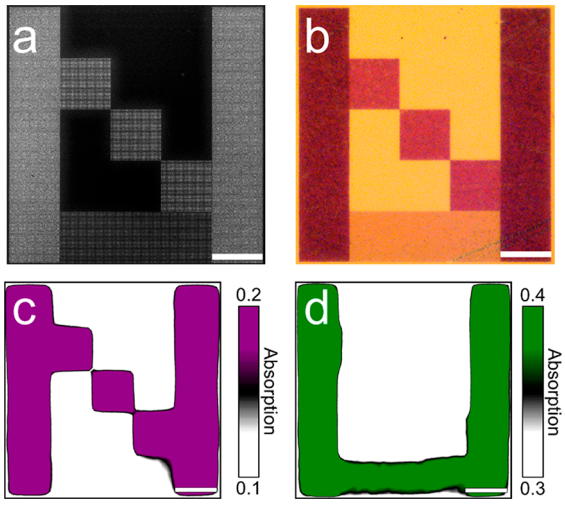

Figure 3. Image decoding at two wavelengths. (a) SEM image showing a surface encoded with two sizes of cubes. (b) Optical image of the same surface. (c,d) Absorption intensity maps of the surface at (c) λ = 773 nm showing the image of letter N formed by cubes with 86 nm edge lengths and (d) λ = 687 nm showing the image of letter U formed by cubes with 63 nm edge lengths. All cube arrays used for encoding have a periodicity of 300 nm. Scale bars are 10 μm.

Cubes with 86 nm in edge length are arranged into the form of a letter N, whereas cubes with 63 nm in edge length are arranged into a letter U. SEM characterization confirmed that nanoparticles were assembled in high yield over all areas. Using a 2 by 2 μm^2 mapping pixel, the absorption spectrum of the surface was measured with an inverted optical microscope (details of mapping setup is described in Supporting Information). Figure 3c,d shows that by comparing the absorption intensity of the surface at different wavelengths, both images in the pattern could be decoded.

In summary, we have shown that DNA-mediated, size-selective assembly can be used to assemble two different sizes of nanocubes on a surface with precise control over the location of the individual nanoparticles. Importantly, this synthetic control enables us to encode surfaces with multiple images in one pattern, which highlights the potential of template-confined nanoparticle assembly for high-resolution multiplexed surface encoding. In addition to encoding the surface via optical absorption intensity, this process could be extended to other encoding signals, such as fluorescence,[8] Raman,[47] or electronic[48] outputs. Indeed, because the size-selective assembly process described here depends only on the size of the particles and the length of the DNA, but not the chemical architecture of the DNA (other than sequence), additional signaling molecules such as dyes could be precisely placed within the DNA shell,[49] opening up new opportunities for sophisticated encoding that provide an even higher density of information.[5]

■ ASSOCIATED CONTENT

Supporting Information

The Supporting Information is available free of charge on the ACS Publications website at DOI: 10.1021/acs.nanolett.8b00509.

Experimental details for nanoparticle synthesis, substrate fabrication, DNA synthesis, purification and functionalization of particles and substrates, nanocube array assembly, optical measurements, and FDTD simulations (PDF)

■ AUTHOR INFORMATION

Corresponding Authors

*E-mail: v-dravid@northwestern.edu.
*E-mail: aydin@northwestern.edu.
*E-mail: chadnano@northwestern.edu.

ORCID

Zizhuo Liu: 0000-0001-5657-8803
Peng-Cheng Chen: 0000-0002-0411-9549
Vinayak P. Dravid: 0000-0002-6007-3063
Koray Aydin: 0000-0002-3268-2216
Chad A. Mirkin: 0000-0002-6634-7627

Author Contributions

⊥Q.-Y.L. and E.P. contributed equally to this work

Notes

The authors declare no competing financial interest.

■ ACKNOWLEDGMENTS

This material is primarily based upon work supported by the Air Force Office of Scientific Research Awards FA9550-12-1-0280 and FA9550 17-1-0348 (nanoparticle assembly). The research was also supported by the Sherman Fairchild Foundation, Inc. (nanoparticle synthesis) and the Center for Bio-Inspired Energy Science, an Energy Frontier Research Center funded by the U.S. Department of Energy, Office of Science, Basic Energy Sciences Award DE-SC0000989 (optical characterizations). K.A. also acknowledges partial support from the Office of Naval Research Young Investigator Program (optical simulations). P.-C.C. also acknowledges support from the Cabell Terminal Year Fellowship from Northwestern University. This work made use of the EPIC facility of the NUANCE Center at Northwestern University, which has received support from the Soft and Hybrid Nanotechnology Experimental (SHyNE) Resource (NSF NNCI-1542205); the MRSEC program (NSF DMR-1121262) at the Materials Research Center; the Keck Foundation, and the State of Illinois, through the IIN.

■ REFERENCES

(1) Taton, T. A.; Mirkin, C. A.; Letsinger, R. L. *Science* **2000**, *289* (5485), 1757−1760.
(2) Pregibon, D. C.; Toner, M.; Doyle, P. S. *Science* **2007**, *315* (5817), 1393−1396.
(3) Braeckmans, K.; De Smedt, S. C.; Leblans, M.; Pauwels, R.; Demeester, J. *Nat. Rev. Drug Discovery* **2002**, *1* (6), 447−456.
(4) Schubert, M.; Steude, A.; Liehm, P.; Kronenberg, N. M.; Karl, M.; Campbell, E. C.; Powis, S. J.; Gather, M. C. *Nano Lett.* **2015**, *15* (8), 5647−5652.
(5) Smith, A. F.; Skrabalak, S. E. *J. Mater. Chem. C* **2017**, *5* (13), 3207−3215.
(6) Kumar, V.; Guleria, P.; Mehta, S. K. *Environ. Chem. Lett.* **2017**, *15* (2), 165−177.
(7) Gooch, J.; Daniel, B.; Abbate, V.; Frascione, N. *TrAC, Trends Anal. Chem.* **2016**, *83*, 49−54.
(8) Wang, Z.; Zong, S.; Li, W.; Wang, C.; Xu, S.; Chen, H.; Cui, Y. *J. Am. Chem. Soc.* **2012**, *134* (6), 2993−3000.
(9) Qin, L.; Banholzer, M. J.; Millstone, J. E.; Mirkin, C. A. *Nano Lett.* **2007**, *7* (12), 3849−3853.

DOI: 10.1021/acs.nanolett.8b00509
Nano Lett. 2018, 18, 2645−2649

(10) Cao, Y. C.; Jin, R.; Mirkin, C. A. *Science* **2002**, *297* (5586), 1536−1540.
(11) Schmucker, A. L.; Dickerson, M. B.; Rycenga, M.; Mangelson, B. F.; Brown, K. A.; Naik, R. R.; Mirkin, C. A. *Small* **2014**, *10* (8), 1485−1489.
(12) Lin, Q.-Y.; Li, Z.; Brown, K. A.; O'Brien, M. N.; Ross, M. B.; Zhou, Y.; Butun, S.; Chen, P.-C.; Schatz, G. C.; Dravid, V. P.; Aydin, K.; Mirkin, C. A. *Nano Lett.* **2015**, *15* (7), 4699−4703.
(13) Myers, B. D.; Lin, Q.-Y.; Wu, H.; Luijten, E.; Mirkin, C. A.; Dravid, V. P. *ACS Nano* **2016**, *10* (6), 5679−5686.
(14) Stewart, J. W.; Akselrod, G. M.; Smith, D. R.; Mikkelsen, M. H. *Adv. Mater.* **2017**, *29* (6), 1602971.
(15) Flauraud, V.; Mastrangeli, M.; Bernasconi, G. D.; Butet, J.; Alexander, D. T. L.; Shahrabi, E.; Martin, O. J. F.; Brugger, J. *Nat. Nanotechnol.* **2016**, *12* (1), 73−80.
(16) Cui, Y.; Phang, I. Y.; Lee, Y. H.; Lee, M. R.; Zhang, Q.; Ling, X. Y. *Chem. Commun.* **2015**, *51* (25), 5363−5366.
(17) Banholzer, M. J.; Qin, L.; Millstone, J. E.; Osberg, K. D.; Mirkin, C. A. *Nat. Protoc.* **2009**, *4* (6), 838−848.
(18) Kuemin, C.; Nowack, L.; Bozano, L.; Spencer, N. D.; Wolf, H. *Adv. Funct. Mater.* **2012**, *22* (4), 702−708.
(19) Liu, Y.; Lee, Y. H.; Zhang, Q.; Cui, Y.; Ling, X. Y. *J. Mater. Chem. C* **2016**, *4* (19), 4312−4319.
(20) Lee, H.; Kim, J.; Kim, H.; Kim, J.; Kwon, S. *Nat. Mater.* **2010**, *9* (9), 745−749.
(21) Lu, Y.; Zhao, J.; Zhang, R.; Liu, Y.; Liu, D.; Goldys, E. M.; Yang, X.; Xi, P.; Sunna, A.; Lu, J.; Shi, Y.; Leif, R. C.; Huo, Y.; Shen, J.; Piper, J. A.; Robinson, J. P.; Jin, D. *Nat. Photonics* **2014**, *8* (1), 32−36.
(22) Kim, J.; et al. *Nanotechnology* **2014**, *25* (15), 155303.
(23) Rycenga, M.; Cobley, C. M.; Zeng, J.; Li, W.; Moran, C. H.; Zhang, Q.; Qin, D.; Xia, Y. *Chem. Rev.* **2011**, *111* (6), 3669−3712.
(24) Xia, Y.; Xiong, Y.; Lim, B.; Skrabalak, S. E. *Angew. Chem., Int. Ed.* **2009**, *48* (1), 60−103.
(25) O'Brien, M. N.; Jones, M. R.; Brown, K. A.; Mirkin, C. A. *J. Am. Chem. Soc.* **2014**, *136* (21), 7603−7606.
(26) Halas, N. J.; Lal, S.; Chang, W.-S.; Link, S.; Nordlander, P. *Chem. Rev.* **2011**, *111* (6), 3913−3961.
(27) Myroshnychenko, V.; Rodríguez-Fernández, J.; Pastoriza-Santos, I.; Funston, A. M.; Novo, C.; Mulvaney, P.; Liz-Márzan, L. M.; García de Abajo, F. *Chem. Soc. Rev.* **2008**, *37* (9), 1792−1805.
(28) Moreau, A.; Ciraci, C.; Mock, J. J.; Hill, R. T.; Wang, Q.; Wiley, B. J.; Chilkoti, A.; Smith, D. R. *Nature* **2012**, *492* (7427), 86−89.
(29) Akselrod, G. M.; Argyropoulos, C.; Hoang, T. B.; Ciraci, C.; Fang, C.; Huang, J. N.; Smith, D. R.; Mikkelsen, M. H. *Nat. Photonics* **2014**, *8* (11), 835−840.
(30) Akselrod, G. M.; Huang, J.; Hoang, T. B.; Bowen, P. T.; Su, L.; Smith, D. R.; Mikkelsen, M. H. *Adv. Mater.* **2015**, *27* (48), 8028−8034.
(31) Hoang, T. B.; Mikkelsen, M. H. *Appl. Phys. Lett.* **2016**, *108* (18), 183107.
(32) Litt, D. B.; Jones, M.; Hentschel, M.; Wang, Y.; Yang, S.; Ha, H. D.; Zhang, X.; Alivisatos, A. P. *Nano Lett.* **2018**, *18*, 859.
(33) Lin, Q.-Y.; Mason, J. A.; Li, Z.; Zhou, W.; O'Brien, M. N.; Brown, K. A.; Jones, M. R.; Butun, S.; Lee, B.; Dravid, V. P.; Aydin, K.; Mirkin, C. A. *Science* **2018**, *359*, 669.
(34) Mason, J. A.; Laramy, C. R.; Lai, C.-T.; O'Brien, M. N.; Lin, Q.-Y.; Dravid, V. P.; Schatz, G. C.; Mirkin, C. A. *J. Am. Chem. Soc.* **2016**, *138* (28), 8722−8725.
(35) Mirkin, C. A.; Letsinger, R. L.; Mucic, R. C.; Storhoff, J. J. *Nature* **1996**, *382* (6592), 607−609.
(36) Jones, M. R.; Seeman, N. C.; Mirkin, C. A. *Science* **2015**, *347* (6224), 1260901.
(37) O'Brien, M. N.; Radha, B.; Brown, K. A.; Jones, M. R.; Mirkin, C. A. *Angew. Chem., Int. Ed.* **2014**, *53* (36), 9532−9538.
(38) Ku, J. C.; Ross, M. B.; Schatz, G. C.; Mirkin, C. A. *Adv. Mater.* **2015**, *27* (20), 3159−3163.
(39) Wang, M. X.; Seo, S. E.; Gabrys, P. A.; Fleischman, D.; Lee, B.; Kim, Y.; Atwater, H. A.; Macfarlane, R. J.; Mirkin, C. A. *ACS Nano* **2017**, *11* (1), 180−185.
(40) Xie, Z.; Gordiichuk, P.; Lin, Q.-Y.; Meckes, B.; Chen, P.-C.; Sun, L.; Du, J. S.; Zhu, J.; Liu, Y.; Dravid, V. P.; Mirkin, C. A. *ACS Nano* **2017**, *11* (8), 8231−8241.
(41) Zhou, X.; Zhou, Y.; Ku, J. C.; Zhang, C.; Mirkin, C. A. *ACS Nano* **2014**, *8* (2), 1511−1516.
(42) Zhou, Y.; Zhou, X.; Park, D. J.; Torabi, K.; Brown, K. A.; Jones, M. R.; Zhang, C.; Schatz, G. C.; Mirkin, C. A. *Nano Lett.* **2014**, *14* (4), 2157−2161.
(43) Kuemin, C.; Cathrein Huckstadt, K.; Lörtscher, E.; Rey, A.; Decker, A.; Spencer, N. D.; Wolf, H. *Adv. Mater.* **2010**, *22* (25), 2804−2808.
(44) Siavoshi, S.; Yilmaz, C.; Somu, S.; Musacchio, T.; Upponi, J. R.; Torchilin, V. P.; Busnaina, A. *Langmuir* **2011**, *27* (11), 7301−7306.
(45) Zhou, Y.; Zhou, X. Z.; Park, D. J.; Torabi, K.; Brown, K. A.; Jones, M. R.; Zhang, C.; Schatz, G. C.; Mirkin, C. A. *Nano Lett.* **2014**, *14* (4), 2157−2161.
(46) Cowie, J. M. G.; Mohsin, M. A.; McEwen, I. J. *Polymer* **1987**, *28* (9), 1569−1572.
(47) Banholzer, M. J.; Millstone, J. E.; Qin, L.; Mirkin, C. A. *Chem. Soc. Rev.* **2008**, *37* (5), 885−897.
(48) Yang, C.; Zhong, Z.; Lieber, C. M. *Science* **2005**, *310* (5752), 1304−1307.
(49) Park, D. J.; Ku, J. C.; Sun, L.; Lethiec, C. M.; Stern, N. P.; Schatz, G. C.; Mirkin, C. A. *Proc. Natl. Acad. Sci. U. S. A.* **2017**, *114* (3), 457−461.

DOI: 10.1021/acs.nanolett.8b00509
Nano Lett. 2018, 18, 2645−2649